Analysis of transport properties of tetrahertz quantum cascade lasers

Hans Callebaut, Sushil Kumar, Benjamin S. Williams, and Qing Hu[a)]
Department of Electrical Engineering and Computer Science and Research Laboratory of Electronics, Massachusetts Institute of Technology, Cambridge, Massachusetts 02139

John L. Reno
Sandia National Laboratories, Department 1123, MS 0601, Albuquerque, New Mexico 87185-0601

(Received 21 January 2003; accepted 9 May 2003)

We present a self-consistent modeling of a 3.4-THz intersubband laser device. An ensemble Monte Carlo simulation, including both carrier–carrier and carrier-phonon scattering, is used to predict current density, population inversion, gain, and electron temperature. However, these two scattering mechanisms alone appear to be insufficient to explain the observed current density. In addition, the insufficient scattering yields a gain that is slightly higher than inferred from experiments. This suggests the presence of a non-negligible scattering mechanism which is unaccounted for in the present calculations. © *2003 American Institute of Physics.* [DOI: 10.1063/1.1590749]

Over the past several years, the quantum cascade laser (QCL) has proven to be a very successful source for mid-infrared and, more recently, far-infrared [terahertz (THz)] coherent radiation.[1–3] Despite their many similarities, mid- and far-infrared QCLs show a qualitative difference in the dynamics of electron transport. For mid-infrared QCLs, the radiative transition energy $\hbar\omega$ exceeds the longitudinal optical (LO) phonon energy $\hbar\omega_{\mathrm{LO}}$ and electron transport is dominated by LO-phonon scattering. In the THz frequency range, where $\hbar\omega<\hbar\omega_{\mathrm{LO}}$, only the high-energy tail of a hot electron distribution is subject to the LO-phonon scattering, which results in a significantly higher temperature sensitivity for the electron transport and a far greater importance of electron–electron (e–e) scattering. The long delay in the development of THz QCLs is testimony to the difficulty of achieving population inversion involving these complicated transport mechanisms. It is thus important to quantitatively model these transport processes to extend the operation of THz QCLs to broader frequency ranges and higher temperatures.

Our transport analysis is based on Monte Carlo (MC) simulations, which have been used to analyze and design mid-infrared and THz QCLs.[4,5] Compared to conventional rate-equation analysis, the MC method is especially useful for THz QCLs, as it does not rely on a specific model for carrier distributions and can easily handle temperature- and density-dependent scattering times. The MC simulation follows a conventional scheme for an ensemble of particles,[6,7] with a focus on e–e and electron-phonon interactions involving the electrons in one module of the device under study. Only interactions with electrons in states belonging to the same or a neighboring module are considered. An electron that scatters out of a module is reinjected with identical in-plane wavevector into a subband equivalent to its destination subband, in accordance with the spatial periodicity of the QCL.[4] The e–e interactions include dynamic screening[8] and were implemented based on the scheme outlined by Goodnick and Lugli,[7] with the correction by Mosko *et al.*[9] This correction, which we have verified both analytically and numerically, results in a factor-of-4 lower e–e scattering rate than in Refs. 6 and 7. Due to the relatively low Al content in the simulated GaAs–AlGaAs structures, the use of bulk LO-phonon scattering rates is a good approximation.[10] Both acoustic and hot-LO-phonon scattering, including emission and absorption processes, were included in the simulations. A time constant of $\tau=5$ ps was assumed for the decay of LO phonons into acoustic phonons. The acoustic phonons are assumed to follow a Bose–Einstein distribution at the lattice temperature. No phenomenological parameters were introduced.

It should be noted that some qualitative issues still remain, particularly concerning wavefunction coherence and localization. In the present MC model, the Schrödinger equation is solved for a band structure profile spanning several modules, yielding a fully coherent picture of the subbands and the corresponding wavefunctions. No model for localization resulting from dephasing scattering was implemented. Consequently, for certain narrow bias ranges, even weakly coupled subbands (characterized by a small anticrossing gap between these levels) can interact and give rise to unrealistic spatially extended states. The parasitic current channels resulting from these anticrossings are usually easily identifiable, as they appear as a sharp current spike in a very narrow bias range, because fast LO-phonon scattering is now allowed to lower-energy states which are located far away. In reality, dephasing scattering[11] reduces the coupling between different subbands, effectively eliminating the coherent interaction between weakly coupled states. This leads to more localized states and a decrease in electron transport and, hence, a lower current density than calculated using the fully coherent model. However, close to anticrossing, transport between weakly coupled states could still significantly influence current density and electron dynamics. In the absence of dephasing scattering in the simulation, the narrow current spikes due to these parasitic channels were largely disregarded. Only current spikes due to subbands with a larger anticrossing gap (>0.5 meV) were investigated further. The decreased wavefunction coherence in a calculation including

a)Electronic mail: qhu@mit.edu

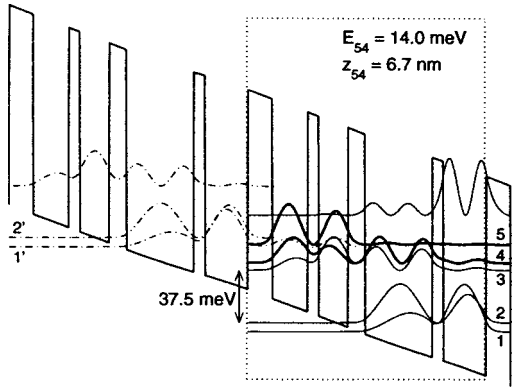

FIG. 1. Band structure and key intersubband energy separations for the simulated structure. Also indicated is the dipole moment for the radiative transition. The device consists of GaAs/$Al_{0.15}Ga_{0.85}As$ layers with thicknesses (nm) **5.4**/7.8/**2.4**/6.4/**3.8**/14.8/**2.4**/9.4 (barriers in boldface, wells in plain text) and is doped to $n=1.9\times10^{16}$ cm^{-2} in the 14.8 nm wide well.

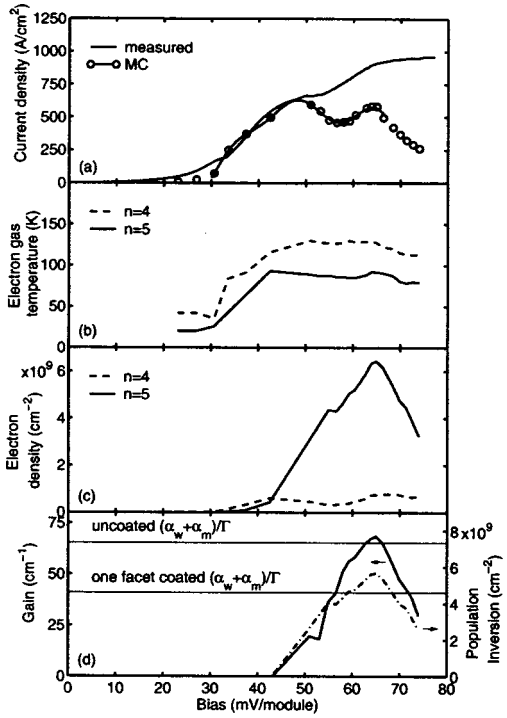

FIG. 2. Key results of the MC simulation for a lattice temperature of 25 K. (a) Current density for a range of biases. The injection anticrossing occurs at 65 mV/module. A tenth-order polynomial fit provides a guide to the eye. The measured current density is represented as a full line. The large parasitic current peak of $\sim$2000 A/cm^2 at $\sim$45 mV/module was omitted from the calculation results. (b) $T_{\rm el}$ for the subbands involved in the radiative transition, $n=4$ and $n=5$. (c) The population density in $n=4$ and $n=5$. (d) Material gain for different biases. To first order, the gain is proportional to the population inversion. Also indicated are the calculated threshold gain values for a 1180×150 μm^2 ridge structure, with uncoated facets and with one facet made fully reflecting.

dephasing will most likely result in a decline in carrier transport and current density, which means that the code as implemented overestimates the current density.

The main focus of our simulations is a 3.4-THz QCL,[3] as shown in Fig. 1. Electrons, injected from $n=1'$ into $n=5$, make a vertical radiative transition into $n=4$. The subbands $n=4$ and $n=3$ are in resonance, which enables fast LO-phonon-mediated depopulation into $n=2$ and $n=1$. The simulated structure is in accordance with x-ray diffraction data obtained from the grown sample.

The mean active region temperature was calculated using temperature-dependent values for the heat capacity[12] of the substrate and active region. Due to the heterostructure nature of the GaAs–$Al_{0.15}Ga_{0.85}As$ active region, the thermal conductivity κ in the laser ridge is substantially lower than in a bulk material.[13,14] For a heat sink temperature $T_{\rm sink}=5$ K, the very small low-temperature heat capacity and the low κ in the active region lead to a substantial increase in lattice temperature to $T_{\rm latt}\approx25$ K after a 100-ns pulse. Consequently, a value of $T_{\rm latt}=25$ K was used in all calculations. The results of the MC simulations are summarized in Fig. 2. The measured $I-V$ curve was adjusted to account for a parasitic series resistance of 2 Ω and is reproduced qualitatively by the simulated curve. The first increase in current density occurs in a bias range of $\sim$35–45 mV/module where the injector level $n=1'$ becomes aligned with $n=3$, which is designed to be rapidly depopulated by resonant LO-phonon scattering. The narrow anticrossing gap between these two levels ($\sim$0.6 meV) indicates that the calculated peak current density of nearly 2000 A/cm^2 at $\sim$45 mV/module (not shown) is a severe overestimation. Still, the parasitic channel carries an important amount of current, as is evident from the experimentally observed current shoulder at $\sim$45 mV/module. In order to lower the laser's threshold current density, this parasitic current needs to be reduced significantly. This can be achieved by reducing the coupling between the injector ground state and the upper LO-phonon resonant state by adding more wells to the active or injector regions, or alternatively by increasing the thickness of the barriers between those states.

At biases exceeding 50 mV/module, the $n=2'$ and $n=1'$ doublet injects carriers into the upper radiative level $n=5$, yielding a gain as shown in Fig. 2(d). The injector ground state $n=1'$ and $n=5$ line up at the design bias of 65 mV/module. Some key calculation results for this bias are summarized in Table I. In this letter, all scattering times reflect the net scattering rates, including the effect of backscattering from the final state. For example, for scattering from level i into level f, the effective scattering time τ_{if} is given by

$$\frac{1}{\tau_{if}}=\frac{1}{\tau_{if}^{0}}\left(1-\frac{n_f}{n_i}\frac{\tau_{if}^{0}}{\tau_{fi}^{0}}\right), \tag{1}$$

where n_i and n_f are the population densities for subbands i and f, respectively, and τ_{if}^{0} and τ_{fi}^{0} are the scattering times without the inclusion of backscattering. Note that the calculated electron temperature $T_{\rm el}$ varies by more than 30 K from

TABLE I. Calculated subband energy, electron temperature, population density, and subband lifetime at injection anticrossing, at $T_{\rm latt}=25$ K. $\tau_4=0.55$ ps, $\tau_{54}=13.1$ ps, $\tau_5=3.5$ ps.

n	E (meV)	$T_{\rm el}$ (K)	Pop. (10^{10} cm^{-2})
1	0	102	0.77
2	6.5	111	1.29
3	44.0	122	0.10
4	49.3	133	0.08
5	63.3	96	0.64

subband to subband, depending on how effectively LO-photon scattering cools down the electron gas. This calculation result illustrates that a simple rate equation model with a uniform subband temperature cannot adequately reflect the physics of a THz QCL. Due to the anticrossing with $n=3$, the lower laser level $n=4$ is depopulated efficiently ($\tau_4=0.55$ ps). The predicted high carrier temperature results in an increased LO-phonon scattering in the active region, with $\tau_{54}^{\mathrm{LO}}=18$ ps while $\tau_{54}^{\mathrm{e-e}}=47$ ps. With scattering times $\tau_{1'5}=6$ ps, $\tau_{1'4}=18$ ps and $\tau_{1'3}=13$ ps, the laser suffers from a low injection efficiency of approximately 55%, which contributes to a high threshold current density. By reducing the parasitic $1'\rightarrow 3$ channel, the injection efficiency can be increased to $\sim 75\%$. This would not only be beneficial to the population inversion, but also significantly decrease the power dissipation, lowering the lattice temperature for cw operation by more than 10 K. The resulting drop in electron temperature and nonresonant LO-phonon scattering would further enhance lasing operation temperatures. The gain is given by

$$g=\frac{\Delta N_{54} e^2 f_{54}}{2\pi L_p c n \epsilon_0 m^* \Delta \nu}, \tag{2}$$

where L_p is the length of one module, n is the refractive index, m^* is the bulk effective mass of GaAs, and $\Delta\nu$ is the spontaneous emission linewidth in hertz. Using the measured values[15] for $n=3.8$ and $\Delta\nu=1.03$ THz (4.25 meV), as well as simulated values for the oscillator strength $f_{54}=0.98$ and the population inversion $\Delta N_{54}=5.6\times 10^9$ cm^{-2} at the design bias, a peak gain of 68 cm^{-1} is calculated. This value is an overestimation as wavefunction localization is likely to result in a more incoherent and less efficient electron transport through the injector barrier, diminishing the population inversion and hence the gain. For comparison, we achieved lasing from a 1.18-mm-long Fabry–Pérot ridge with one Au-coated facet (facet loss $\alpha_m=-1/2L\ln R$), but no lasing with both facets uncoated ($\alpha_m=-1/L\ln R$). Hence, the peak gain value is bounded by the total cavity losses of these two structures, shown as the two horizontal lines in Fig. 2(d). In the calculation of the waveguide loss $\alpha_w=7.1$ cm^{-1} and the mode confinement factor $\Gamma=0.29$, a Drude model was used with $\tau=0.5$ ps in the active region and $\tau=0.1$ ps in the contact layers. As shown in Fig. 2(d), the calculated maximum gain slightly exceeds the upper bound of the range inferred from the measured results.

The predicted peak current density of 580 A/cm^2, however, falls well short of the measured 915 A/cm^2. The difference between measurement and simulation is too large to be accounted for by the absence of a minor transport mechanism, and will be even greater if dephasing scattering and wavefunction localization are considered. The same discrepancy appears to be present in simulated results of other devices where e–e scattering plays an important role in the electron transport. For example, for the three-level structure described in Ref. 16, the predicted current density of 110 A/cm^2 is much lower than the measured ~ 300 A/cm^2. Also, for the device described in Ref. 17, the calculated current density of 55 A/cm^2 is less than the reported 105 A/cm^2. On the other hand, carrier transport in the laser described in Ref. 1 is dominated by LO-phonon scattering, because of elevated electron temperatures in the wide (~ 20 meV) injector miniband and the large spatial overlap between the upper laser level and some lower miniband states. In this case our calculated peak current density of 1500 A/cm^2 exceeds the reported 850 A/cm^2. The earlier examples suggest that either a major current path is missing in the present simulation for devices in which e–e scattering plays a major role, or the importance of existing current paths is underestimated.

In conclusion, we have calculated the $I-V$ characteristics and gain of a working THz laser and compared the results with experimental measurements. The sizeable discrepancy in current density suggests the presence of a major scattering mechanism that is yet unaccounted for. Another consequence of this underestimation of scattering is a gain that is slightly higher than inferred from experiments.

The authors would like to thank S. Goodnick for generously allowing us to adapt his MC code. This work is supported by AFOSR, NASA, and NSF. Sandia is a multiprogram laboratory operated by Sandia Corporation, a Lockheed Martin company, for the United States Department of Energy under Contract No. DE-AC04-94AL85000.

[1] R. Köhler, A. Tredicucci, F. Beltram, H. E. Beere, E. H. Linfield, A. G. Davis, D. A. Ritchie, R. C. Iotti, and F. Rossi, Nature (London) **417**, 156 (2002).
[2] M. Rochat, L. Ajili, H. Willenberg, J. Faist, H. Beere, G. Davis, E. Linfield, and D. Ritchie, Appl. Phys. Lett. **81**, 1381 (2002).
[3] B. S. Williams, H. Callebaut, S. Kumar, Q. Hu, and J. L. Reno, Appl. Phys. Lett. **82**, 1015 (2003).
[4] R. C. Iotti and F. Rossi, Appl. Phys. Lett. **76**, 2265 (2000).
[5] R. Köhler, R. C. Iotti, A. Tredicucci, and F. Rossi, Appl. Phys. Lett. **79**, 3920 (2001).
[6] C. Jacoboni and P. Lugli, *The Monte Carlo Method for Semiconductor Device Simulations* (Springer, New York, 1989).
[7] S. M. Goodnick and P. Lugli, Phys. Rev. B **37**, 2578 (1988).
[8] P. F. Maldague, Surf. Sci. **73**, 296 (1978).
[9] M. Mosko, A. Moskova, and V. Cambel, Phys. Rev. B **51**, 16860 (1995).
[10] B. S. Williams and Q. Hu, J. Appl. Phys. **90**, 5504 (2001).
[11] S. Mukamel, *Principles of Nonlinear Optical Spectroscopy* (Oxford University Press, New York, 1995).
[12] J. S. Blakemore, J. Appl. Phys. **53**, R123 (1982).
[13] V. Spagnolo, M. Troccoli, G. Scamarcio, C. Becker, G. Glastre, and C. Sirtori, Appl. Phys. Lett. **78**, 1177 (2001).
[14] J. Capinski, H. J. Maris, T. Ruf, M. Cardona, K. Ploog, and D. S. Katzer, Phys. Rev. B **59**, 8105 (1999).
[15] B. S. Williams, S. Kumar, H. Callebaut, Q. Hu, and J. L. Reno, Electron. Lett. (to be published).
[16] B. S. Williams, B. Xu, Q. Hu, and R. Melloch, Appl. Phys. Lett. **75**, 2927 (1999).
[17] B. S. Williams, H. Callebaut, Q. Hu, and J. L. Reno, Appl. Phys. Lett. **79**, 4444 (2001).